Geotextiles and Geomembranes 34 (2012) 131–143

Contents lists available at SciVerse ScienceDirect

Geotextiles and Geomembranes

journal homepage: www.elsevier.com/locate/geotexmem

Lessons learned from three failures on a high steep geogrid-reinforced slope

Chia-Nan Liu [a,*], Kuo-Hsin Yang [b], Yu-Hsien Ho [a,c], Chia-Ming Chang [c]

[a] Civil Engineering Department, National Chi-Nan University, University Road, Puli, Nantou 545, Taiwan
[b] Department of Construction Engineering, National Taiwan University of Science and Technology, Taiwan
[c] ACE Geosynthetics Inc., Taichung 435, Taiwan

ARTICLE INFO

Article history:
Received 18 July 2011
Received in revised form
7 April 2012
Accepted 22 May 2012
Available online xxx

Keywords:
Reinforced slope
Case history
Failure
Earthquake
Pore pressure

ABSTRACT

An excavated slope that connects the school campus and Tai-21 Road is located on the approaching road to Chi-Nan University in Nantou, Taiwan. The toe portion of this high and steep slope is reinforced by a PET geogrid, with the height of the reinforced zone ranging between 10 meters (m) and 40 m at different sections. A slope failure occurred during construction of the reinforced slope in 1994. A massive failure of the reinforced slope then happened at the 40 m high section when the Chi-Chi (Taiwan) earthquake struck on September 21, 1999. The failure portion was rehabilitated, but another failure of the reinforced slope took place at another 20 m high section after a heavy rainstorm on July 2, 2004. The research herein presents the information and the history of these PET geogrid-reinforced slope failures. We perform extensive field observations and numerical analyses to examine the failure mechanism and causes contributing to these failures. Lessons learned from these case histories, with regard to carrying out a detailed site investigation, selecting permeable materials as backfill, installing drainage systems appropriately and combining the design of a reinforced slope with other types of retaining structures to improve the system global stability, are also discussed.

1. Introduction

Steepened slopes have the advantage of increasing land usage, whereas the typical slope angle is limited by the characteristics of the natural soil's shear strength. Geosynthetic solutions allow for the construction of slopes with steeper angles than a natural soil slope through tensile reinforcement and geosynthetic/soil interactions. They have been applied to reinforce soil slopes all over the world for more than 20 years.

Conventionally, geosynthetic reinforced retaining structures are designed using the three primary design guidelines (FHWA, 2001; AASHTO, 2002; NCMA, 2010). Many design charts and methods (Schmertmann et al., 1987; Leshchinsky and Boedeker, 1989; Jewell, 1991; Ponterosso and Fox, 1999) have also been developed for the design of reinforced slopes. Numerous numerical and physical studies have been conducted to study the behavior, stability and performance of geosynthetic reinforced retaining structures subjected to various conditions, including layered or soft foundation, differential settlement and limited reinforced space (Rowe and Skinner, 2001; Mandal and Joshi, 1996; Viswanadham and Konig, 2009; Leshchinsky et al., 2004), surcharge loadings (Yoo and Jung, 2008; Yoo and Kim, 2004), seismic loadings (Huang et al., 2011), and low permeable backfill (Raisinghani and Viswanadham, 2011). Some literature of field studies reported the successful design and satisfactory performance of this type of structures (Chang et al., 1991; Turner and Jensen, 2005). However, the literature presents and discusses a rather limited number of failure cases in regards to a further understanding of their original design and failure mechanism. (Leonards et al., 1994; Tatsuoka et al., 1995; Collins, 2001; Ling et al., 2001; Borges and Cardoso, 2002; Yoo, 2004; Yoo et al., 2004, 2006, Scarborough, 2005)

This paper presents a history about an excavated steep slope protected by a PET geogrid-reinforced slope. The height of the reinforced portion ranges between 10 meters (m) and 40 m at different sections. A slope failure occurred during construction of the reinforced slope in 1994, followed by a massive failure of the reinforced slope at a 40 m high section after the Chi-Chi earthquake struck on September 21, 1999. This case attracted a lot of attention in the literature (Chen et al., 2000; Chou and Fan, 2000; Huang, 2000; Holtz et al., 2001). Another failure of the reinforced slope took place at another 20 m high section after a heavy rainstorm on July 2, 2004.

It is interesting to present the series of failures for this reinforced slope. This research conducts a comprehensive study to identify possible causes for these collapses, including extensive field observation, field and laboratory tests of the mechanical

* Corresponding author. Tel.: +886 49 2918084.
E-mail address: cnliu2009@gmail.com (C.-N. Liu).

0266-1144/$ – see front matter © 2012 Elsevier Ltd. All rights reserved.
doi:10.1016/j.geotexmem.2012.05.003

properties of construction materials, slope stability analyses based on the built-in design, and ground motion or pore water pressure estimated from practical earthquake or rainfall data in the field. Finally, the lessons learned from this case study are discussed.

2. Design and construction of the reinforced slope

Chi-Nan University (NCNU) is in central Taiwan on tableland above nearby Taiwan Highway 21 (Tai-21). This tableland is composed of several meters of thick, fully weathered, cohesive, fine-grained particles on the surface and less weathered, coarse-grained pebbles and boulders underneath. Following NCNU's establishment in the early 1990s, a 1220-m long approach road was constructed to connect Tai-21 and the campus by excavating along the surface of the tableland. The pre-construction topography at the site consisted of a relatively gentle natural slope (28°) that dropped from the campus to Tai-21 by a difference in elevation of about 80 m. The excavation of the approach road resulted in a steeper grade. As the tableland slope was cut steep and high at the end of Tai-21 for the approach road, a 430 m long geogrid-reinforced slope was constructed in order to stabilize and landscape the excavated slope. The construction of this reinforced slope began in 1994 and finished in the spring of 1996. The height of reinforced slope zone ranged from 10 m to 40 m, depending on the location and the slope height along the approaching road. Fig. 1 shows an overview of the completed reinforced slope.

Fig. 2a shows a typical slope profile at Section A-A, which consists of four tiers of reinforced slope underlying an unreinforced soil slope. The unreinforced slope, inclined at about 40°, was built by trimming the pre-construction natural slope. The reinforced slope at Section A-A is 40 m high with a slope angle of 63° (1H:2V). The height of each reinforced slope tier is 10 m and the offset distance is 3 m. The backfill material was taken from the field and compacted in each 1 m lift. The vertical spacing between reinforcement layers is 1 m. There are in total forty layers of reinforcement in this section of reinforced slope. The reinforcement lengths, from the bottom tier to up tier of reinforced slope, are 13, 10, 7, and 4 m in sequence.

Two types of geogrids were used as reinforcement. Type-I geogrid, placed in the bottom tier of the reinforced slope, was made of woven polyester fibers with rectangular apertures of 90 millimeters (mm) by 7 mm with a percent open area of 36%. The vendor provided ultimate tensile strength and design tensile strengths of type-I PET geogrids at 260 and 104 kN/m, respectively. Type-II geogrid was placed in the upper three tiers of reinforced slope and was also made of woven polyester fibers with square apertures of 20 mm by 20 mm with percent open area of 64%. Its vendor provided ultimate tensile strength and design tensile strength of 150 and 48 kN/m, respectively. The surface of the reinforced slope was designed to be vegetated and flexible by using PET geogrid wrapped around the compacted backfill layers. The wraparound length was 1.7 m. Due to a gentler slope inclination, three tiers and two tiers of reinforced slope were correspondingly designed at Sections B-B and C-C. The heights of the reinforced slopes are shorter at 30 m and 20 m, respectively. The geometry and configuration of reinforced slope in these sections were similar to those of the upper tiers for Section A-A. Only Type-II geogrid was applied in these sections.

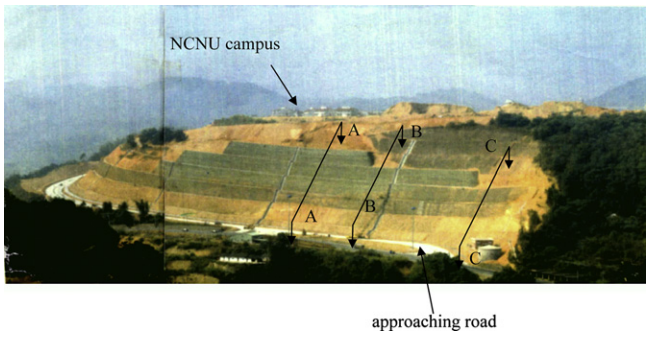

Fig. 1. Overall view of the completed reinforced slope.

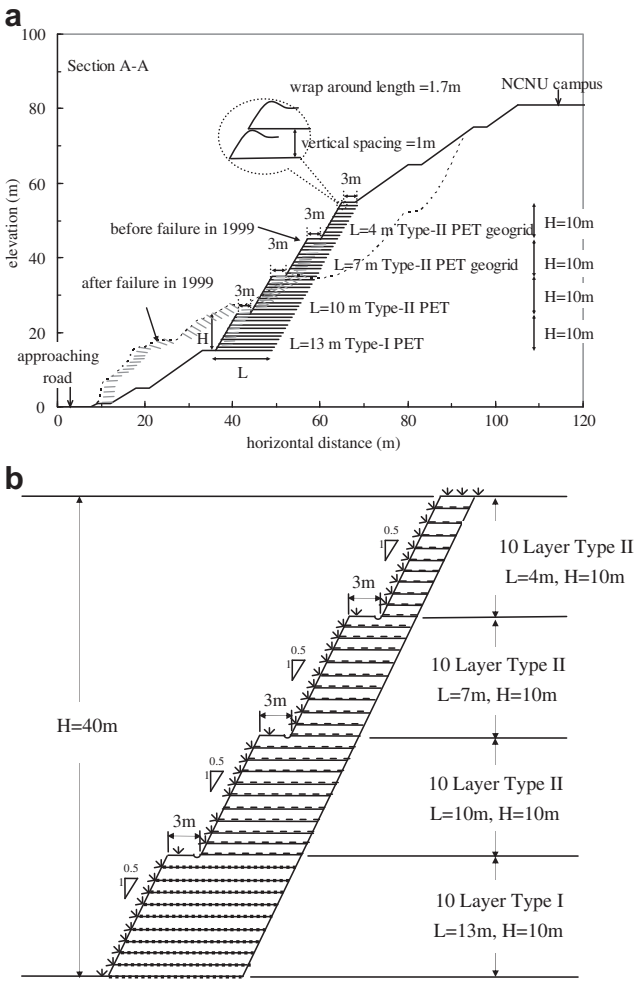

Fig. 2. Slope profile at Section A-A: (a) detailed information; (b) original design.

According to the original design (Fig. 2b), drainage channels were constructed along the slope to route the surface water collected by the drainage channels installed across the offset between the tiers of reinforced zone. We note that there was no subdrainage medium (such as geosynthetics and coarse gravels) installed within or at the boundary of the reinforced zone to collect, control, and drain ground water and seepage out of the reinforced zone.

3. Description of failures

Three failures have occurred on this reinforced slope. The first slope failure occurred during construction in 1994. A second massive failure of the reinforced slope took place after a strong earthquake struck nearby in 1999. The third failure of the reinforced slope happened after a heavy rainfall in 2004. Fig. 3 shows the locations of these failures. This section presents the

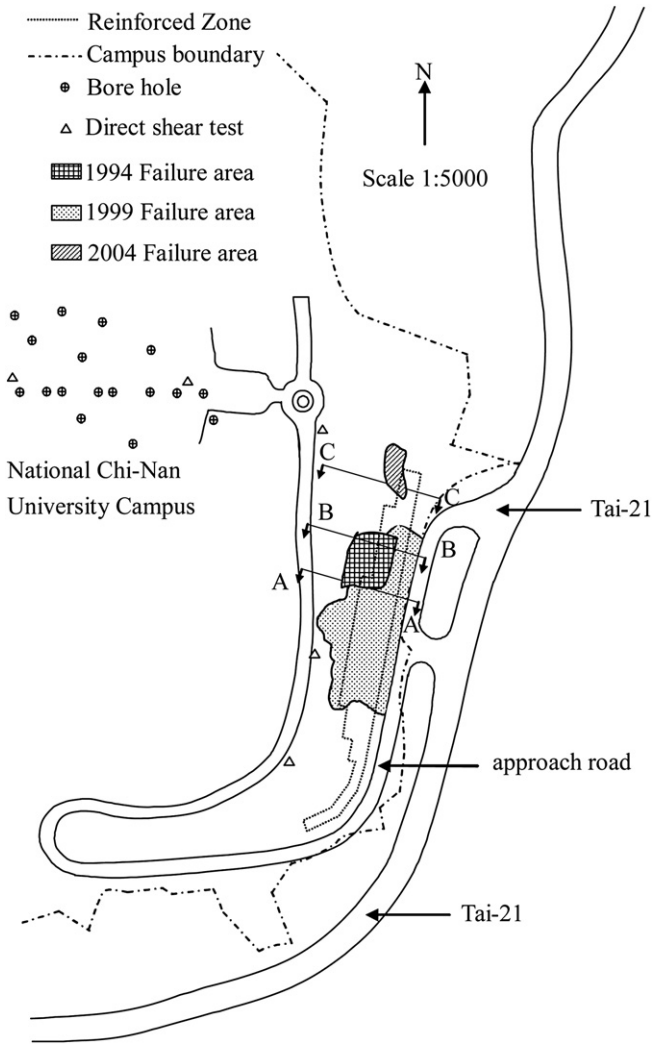

Fig. 3. Plain view of the three failures of reinforced slopes.

descriptions of these failures, including field observation, failure mechanism, and relevant information.

3.1. Slope failure in 1994

The slope failure on November 15, 1994 occurred during construction of the reinforced slope and after a heavy rainfall season. The nearby precipitation station recorded monthly rainfalls for July through October that year of 638.5, 267.5, 173.9, and 81.7 mm, respectively. Failure occurred after construction was completed at the bottom tier of reinforced slope. When the natural soil was excavated to place geogrid and backfill to construct the upper tiers of reinforced slope, a wedge of lateritic gravel slid down along a planar surface (Fig. 4). This sliding plane extended behind the designed reinforced zone up to the mid-height of the natural soil. The sliding material sheared out the upper part of the finished reinforced zone. The bottom tier of reinforced slope, located below the sliding plane, did not shear and remained basically intact.

The sliding plane was along the interface of laterite gravel and underneath stiff brown-yellowish clay. As seen in Fig. 4, it is evident that the failure was closely related to the clay layer. We note that the existence of this clay layer was not shown on any design reports of this reinforced slope. For example, as shown in Fig. 5, the clay layer was not taken into consideration when conducting the original stability analysis of the four-tiered reinforced slope.

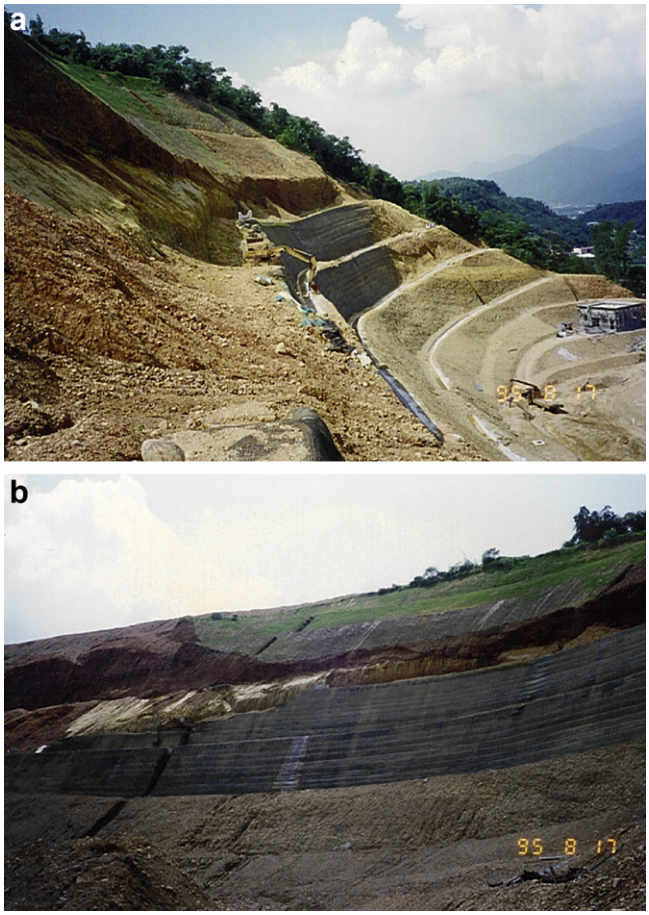

Fig. 4. Failure of reinforced slope at Section A-A during construction in 1994: (a) side view; (b) front view.

This failure postponed the construction of this reinforced slope for more than 14 months in order to resolve difficulties in liability disagreement and rehabilitation. It is important to point out that the construction of this slope still followed the original design, even after a layer of clay not identified earlier was discovered after this failure.

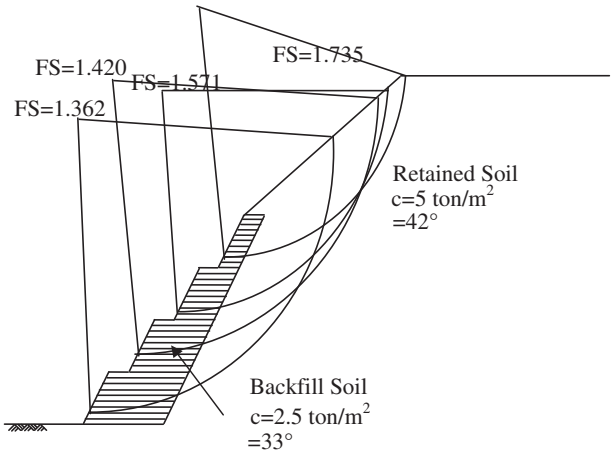

Fig. 5. Original stability analysis for the 4-tiered reinforced slope. Note that the clay layer was not included into analysis.

3.2. Slope failure in 1999

The disastrous 7.3 Chi-Chi earthquake on September 21, 1999, with the epicenter only 20 km away from the NCNU campus in central Taiwan, resulted in a massive failure of the reinforced slope. The time histories of ground accelerations during Chi-Chi earthquake were recorded at Station TCU074 by the National Center for Research on Earthquake Engineering. Station TCU074 is the nearest earthquake observation station to the reinforced slope about 6 km from the slope and 25 km from the epicenter. The recorded peak vertical as well as two peak horizontal ground accelerations in the E–W and S–N directions at Station TCU074 was 273, 380, and 603 gals, respectively. These ground accelerations were much greater than the construction regulated value (i.e., 230 gals) in central Taiwan at that time. Since Chi-Chi Earthquake happened, the regulated value of design ground acceleration has been increased to 330 gals.

Approximately, an area of 180 m in length by 70 m in height slid down toward the approaching road. The profile after failure at Section A-A is shown in Fig. 2, in comparison with the profiles before failure. The entire four-tiered reinforced slope slid down. An apparent scarp (Fig. 6a), at more than 40 m in elevation, was observed in the natural soil slope located near the slope crest (NCNU campus).

A careful field investigation was conducted to examine the reinforcement, with Fig. 6b presenting a close view of the failure at the slope's foot near Section A-A. Though the slide was over 20 m in elevation and 15 m in horizontal distance, most of the geogrid-reinforced layers in the upper three tiers remained intact, though there were gaps between them. These geogrid reinforcements were not horizontal as constructed, but rather rotated upslope at a small angle (as shown in Fig. 2). The extrusion of wrapped-around geogrid at some portion can be seen in Fig. 6b, especially at the bottom tier of the reinforced slope. This happened likely due to the large shear force from the sliding soil mass to extrude the wrapped-around geogrid out. Backfills collapsed and slid toward the slope's toe. About 4–5 layers of reinforced slope in the bottom level were not exposed, but they were buried by the geogrid reinforcement that slid down from upslope. No signs of rupture of the geogrid, nor piping, seepage, or moisturized soil were observed in the field. As seen in these photos, the reinforced zone and natural slope slid down along a significant failure surface, which was within the natural soil retained by the reinforced slope. This leads to a conclusion that the failure was closely related to global instability.

In addition, most of the three-tiered reinforced slope (Section B-B) slid down to a less extent, usually less than 3 m. The sliding surface also extended into the natural soil slope, but the scarp was not so significant. The other portions, including the two-tiered and one-tiered reinforced slopes, basically remained stable (Fig. 6).

The rehabilitation of this failure began in 2002 and was finished in the spring of 2004. Fig. 7 shows countermeasures, including removing the debris of the slide, tapering the slope inclination to 27–34°, soil nailing, and placing a reinforced retaining wall at the slope's toe. The placement of reinforcement material was further examined on site during the rehabilitation. It was found that the overlapping width between geogrids was small, as most did not follow the common standard requirement of 10–30 cm. This defect easily allowed the gap to widen between the geogrid and the backfills to move out between gaps under a lateral loading condition. The embedded length of geogrid was also observed from the failed portion. The measured embedded reinforcement lengths were 30% shorter than the designed lengths. No trace of coarse gravel layer or geosynthetic drainage layer was found when the sliding debris was removed. This observation confirmed that the subdrainage was not installed in the original design of the reinforced slope.

3.3. Slope failure in 2004

The third slope collapse happened after July 2, 2004 when Typhoon Ming-Du-Li passed over Taiwan. Heavy rainfall (maximum hourly rainfall intensity of 166.5 mm and 1-day rainfall accumulation of 503 mm) was recorded at a nearby precipitation station. Fig. 3 presents the location of the failure, which occurred at

Fig. 6. Failure of reinforced slope at Section A-A due to 1999 Chi-Chi earthquake: (a) overall view; (b) close view.

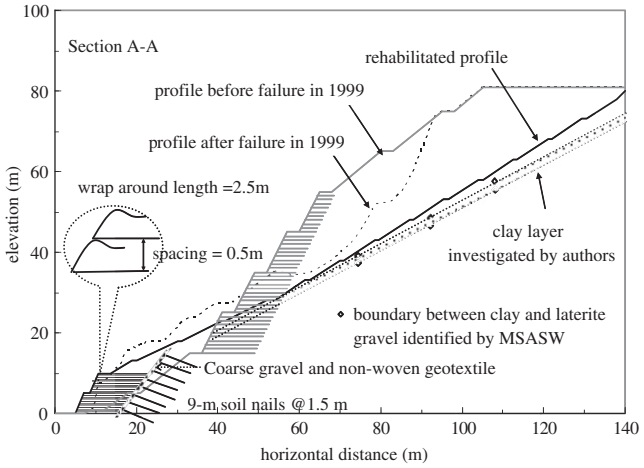

Fig. 7. Designed, failed and rehabilitated profiles for Section A-A with location of clay layer.

the point where two tiers of reinforced slope (Section C-C) were constructed and a nearby natural slope. This portion did not fail in the 1999 Chi-Chi earthquake. An area of about 30 m length by 15 m height slid down (Fig. 8a). A scarp that initiated from the geosynthetic reinforcement-retained natural soil was observed. The sliding material sheared out the upper tier of the reinforced zone and pushed it down. Similar to the slope failure in 1994, the bottom tier of the reinforced slope located below the sliding plane did not shear and remained basically intact (Fig. 8b). A moisturized brown-yellowish clay was also observed along the sliding plane (Fig. 8c). These observations lead to the conclusion that this failure was closely related to rainfall and the clay layer. The rehabilitated portions such as Sections A-A and B-B performed well during this rainstorm.

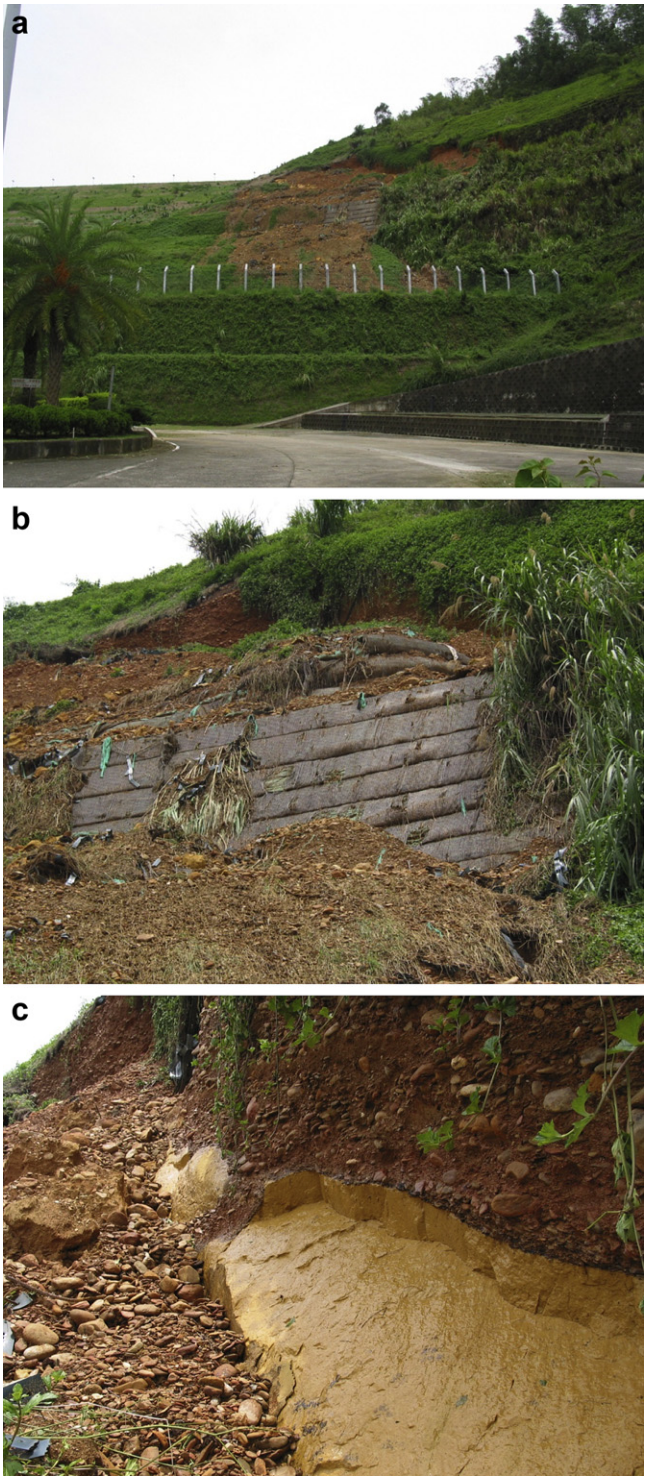

Fig. 8. Failure of reinforced slope at Section C-C due to typhoon induced heavy rainfall in 2004: (a) overall view; (b) close view; (c) clay layer observed along sliding plane of failure.

4. Geological conditions

To collect regional geological information for designing and constructing the NCNU campus buildings and approaching road, 17 boreholes and 5 direct shear field tests were conducted in 1993. Fig. 3 shows the locations of boreholes and field tests. All the boreholes are concentrated at the flat top of the tableland where most buildings are located. The soil stratification of this tableland is plain. From the ground surface down, the tableland consists of a 2–4 m fully weathered laterite topsoil layer with a thick, less weathered laterite soil to gravel layer mixed with sand underneath. A thin (2–10 m) layer mixed with hard clay and gravel is occasionally found at about 15 m below ground surface. According to the experience of drilling a pumping well at Chi-Nan University, the ground water level is very deep at more than 100 m below the tableland surface.

It is observed that no site explorations or field strength tests were specifically conducted for the design and construction of the reinforced slope. Though a thin layer of clay was mentioned on the exploration report, it did not appear on any design documents. The observation after failures led to an apparent conclusion that these failures were closely related to this clay layer. Therefore, several investigations were conducted by the authors to identify its location, thickness, dip, and any diverse effect on the stability of this reinforced slope.

Aside from the information obtained from the failure surface as mentioned in the previous section, a trace of clay layer was monitored during rehabilitation of the 1999 failure when sliding debris was removed and slope inclination was pruned. Multi-station spectral analysis of surface wave (MSASW) tests was conducted on the reconstructed slope surface along elevations of 40, 50, and 60 m above the approaching road in the spring of 2005. Because shear wave velocity is faster in a laterite gravel layer than that in a clay layer, the location of the clay layer is identified as that which has a smaller shear wave velocity. Fig. 9 shows the measured shear wave velocities for different depths at Section A-A. It is observed that a thin layer of lower values exists along this shear

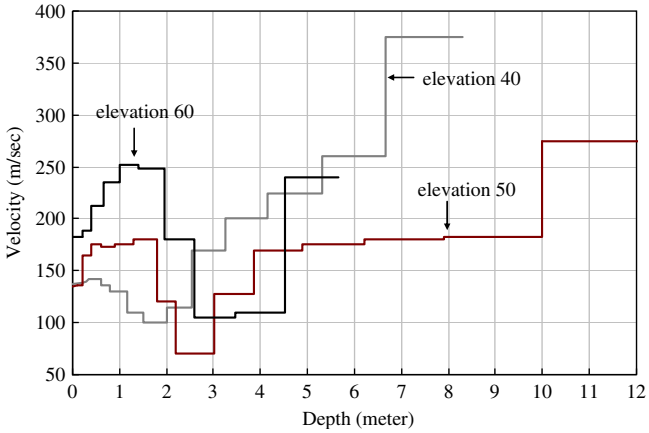

Fig. 9. Shear wave velocity distribution along depth at Section A-A of rehabilitated slope.

wave velocity profile. The boundary between laterite gravel and clay can be easily identified as that point where there is an abrupt change of shear wave velocity. The depth of the clay layer at Section A-A is about 0.5–2.5, 1.8–3.9, and 2.0–4.5 m, respectively, at elevations of 40, 50, and 60 m. By extrapolating these points, the position of the clay layer at Section A-A is shown in Fig. 7. This clay layer has approximately a strike of N25° E and a dip of about 30° to the east. The locations of clay estimated based on the MSASW test results and from field observations of failure and rehabilitation are generally comparable.

5. Engineering properties of construction material

The soil in the retained zone and in the backfill zone of the 1999 failure site was taken for index property tests. Laterite gravel made up 70% of the retained zone by weight, ranging in size from 1 to 20 cm. The fine contents of the soil were medium to high plasticity, with a liquid limit of 53, a plastic limit of 29, and natural moisture contents of 11. In its natural moisture content, the fine content conglomerated together to form a stiff mass several centimeters in size, but this mass dissolved into finer particles under an increase in water content. The soil in the backfill zone contained more fines at about 42% by weight. Some gravel larger than 15 cm in diameter were observed in backfill zone. The field density in retained zone and in backfill zone was estimated by excavating a test pit at undisturbed stratification 0.5 m below the ground surface. The field density was quite high in retained zone while it was significantly lower in the backfill zone. The total unit weights of soil in the retained zone and backfill zone were 22 and 18 kN/m^3, respectively. The compaction of backfill soil was poor corresponding to the degree of compaction about 80%.

Table 1 summarizes the mechanical properties of soils in the backfill zone, retained zone, and clay layer. The soil strength parameters were estimated from large-scale (45 × 45 × 13 cm) drained direct shear test results, while hydraulic conductivity was estimated from permeability tests. In conducting these tests, the test specimen was reconstituted by removing large particles (greater than 2.5 cm) to conform to the common ratio of specimen size to maximum particle size, while the percentage of fine particle, water content, and total unit weight remained the same as in the field. The estimated internal friction angles and cohesion intercepts for soil in the backfill zone and in the retained zone were 28°, 54 kPa and 49°, 13 kPa, respectively. The higher cohesion value from the backfill soil is thought to represent apparent cohesion, considering the partially saturated nature of more fines. The lower friction angle of backfill soil also corresponds to the effects of higher percentage of fines. The hydraulic conductivity of soil in the retained zone and in the backfill zone was in the order of 10^{-3} and 10^{-7} cm/s, respectively. Again, the low hydraulic conductivity in the backfill zone was due to the rather high content of fines. Hung (1978) pointed out that the engineering properties of gravelly laterite are dominated by the laterite soil, because the weight percentage of laterite fine is more than 30%. The internal friction angles and cohesion intercepts for laterite gravel/clay interfaces were also estimated by conducting large-scale direct shear test results. In conducting these tests, the test specimen was also reconstituted to simulate water content and total unit weight in the field. The strength parameters for dry and wet laterite gravel/clay interfaces were 28.5°, 20 kPa and 28.5°, 0 kPa, respectively.

Table 1
Mechanical properties of soils.

Soil	γ_t (kN/m^3)	ϕ' (°)	c' (kPa)	K (kPa)	G (kPa)	k (cm/s)
in Backfill zone	18	28	54	9444	3148	10^{-7}
in Retained zone	22	49	13	56,612	26,129	10^{-3}
Clay layer	20	30	48	29,412	11,280	–
Laterite gravel/clay interface-dry	–	28.5	20	–	–	–
Laterite clay/clay interface-wet	–	28.5	0	–	–	–

Table 2
Mechanical properties of geogrids.

Geogrid type	t (m)	J (kN/m)	T_{ult} (kN/m)	K_s (kN/m^3) for different σ_n (kPa)			c_a (kPa)	δ (°)
				50	100	200		
I	0.0017	4830	126	3865	4910	6889	6.9	40.9
II	0.0014	5128	77	4054	5314	7080	52	44.4

Two types of geogrid were also sampled from the 1999 failure site to conduct an in-isolation wide-width tension test and large-scale direct shear tests of the geogrid/laterite gravel interface. Table 2 lists the engineering properties of these geogrids. The peak tensile strengths of Type-I and Type-II geogrids measured from the tension tests are 126, and 77 kN/m respectively, which are greater than the designed strength (104 and 48 kN/m, respectively) and are about 50% of the nominate ultimate tensile strength (260 and 150 kN/m, respectively) provided by the geogrid manufacturer. It is noted that the measured tensile strength was for the geogrid recovered from the 1999 failure site, which at that time was under the effects of construction, a 3-year creep and environmental degradation, and a high magnitude of cyclic loading. This test results indicate that a value of 2–3 is approximately appropriate as a reduction factor for the allowable long-term design strengths of reinforcements.

6. Numerical analyses

In this section, the failure mechanisms of the reinforced slopes are analyzed using both limit equilibrium and finite difference analyses. The objective of limit equilibrium analyses is to evaluate the stabilities of the reinforced slopes (i.e., calculate the factor of safety) and to locate the failure surfaces on the reinforced slopes. Limit equilibrium analyses were conducted using the Simplified Bishop method with circular surfaces as coded in a commercial design/analysis program, ReSSA, which was developed based on the FHWA design approaches for reinforced slopes. The physical and mechanical properties of soils and reinforcements in the reinforced slope system, presented in the Tables 1 and 2, were adopted in the stability analyses. Unlike the recommended use of allowable tensile strength in the conventional analysis, the limit equilibrium analyses in this study did not consider reduction factors due to installation damage, creep or degradation (i.e., all reduction factors were 1.0). Reduction factors were excluded

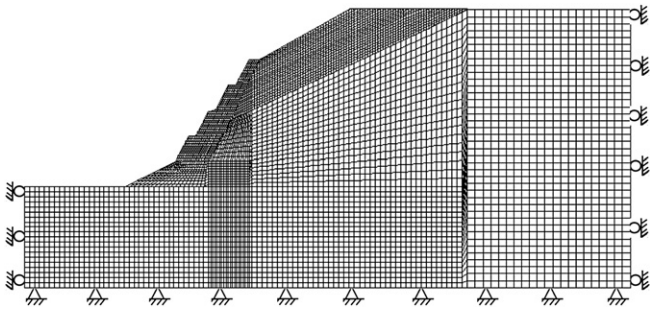

Fig. 10. Finite difference mesh used for modeling Section A-A.

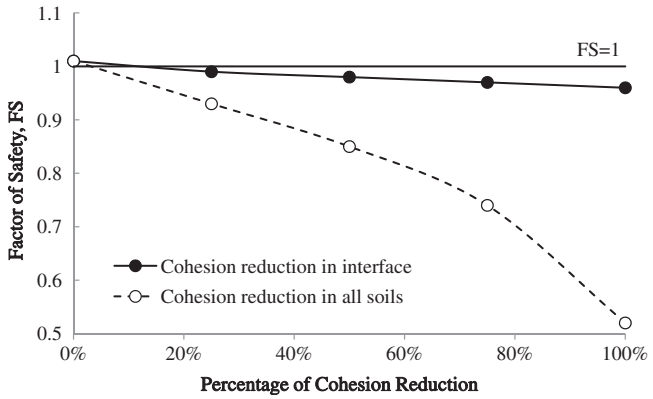

Fig. 11. Variation of FS with different percentages of soil cohesion reduction for the 1994 slope failure at Section A-A.

because these effects have been implicitly included in the input value of reinforcement tensile strength, as discussed previously.

Finite difference analyses were conducted using FLAC (2000) with the aim at gaining insight into the deformation behavior of the reinforced slope system. Information of soil stress, strain and pore water pressure were evaluated by finite difference analyses. In the finite difference simulation, the geogrid was modeled by using a cable element, and its stress–strain behavior was assumed to be elastic. The stress–strain relationship for the soil was an elasto-plastic behavior. The hyperbolic model (Duncan et al., 1980) was applied to modify the elastic modulus after considering the confining pressure and the Mohr–Coulomb model was adopted for describing the plastic behavior. Fig. 10 presents the meshes simulating Section A-A used for numerical analysis. Fixed boundaries were set wide enough from the reinforced slope to eliminate any possible boundary effect under the static loading condition (Lee, 2000), but free boundaries were set to eliminate reflection from a boundary under dynamic loading. One can refer details of the parameter values and manipulation of the FLAC analyses in Jiang (2006). In addition, San et al. (1994) conducted a comparison of finite element analysis of a reinforced slope with the results of a rigorous limit equilibrium analysis. They found the failure of the soil structure can be defined as a state of a rapid increase in strain. Accordingly, in this study, the development and distribution of

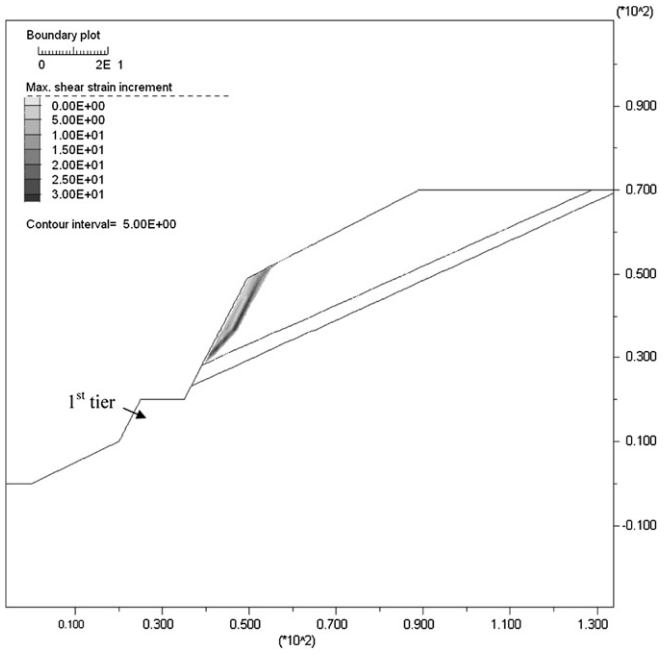

Fig. 13. Finite difference results of the 1994 slope failure at Section A-A at wet condition.

strain increment within the slopes obtained from finite difference analyses were used to identify the stability state and to locate the critical failure surface.

6.1. Results of 1994 slope failure analyses

The field observation indicates that the failure was strongly related to the clay layer. Since the hydraulic conductivity of the laterite gravel in the natural slope was high (10^{-3} cm/s), the rainfall could easily have infiltrated into the slope and absorbed by soil. This moisture migration and absorption likely caused the reduction of soil shear strength and the loss of apparent cohesion from unsaturated soil. This can be justified by the difference of measured gravel/clay interface cohesion under dry and wet conditions. Accordingly, limit equilibrium analyses were conducted to analyze

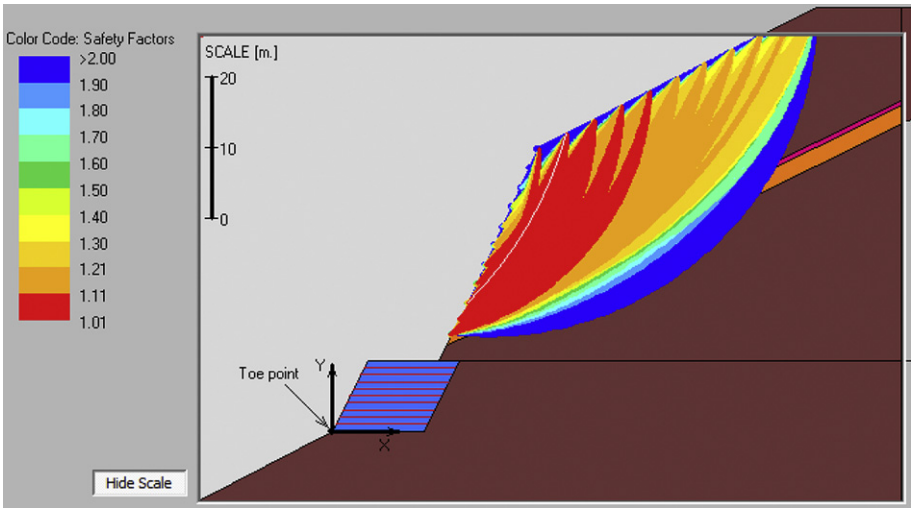

Fig. 12. FS contour and the most critical failure surface of the 1994 slope failure at Section A-A at dry condition.

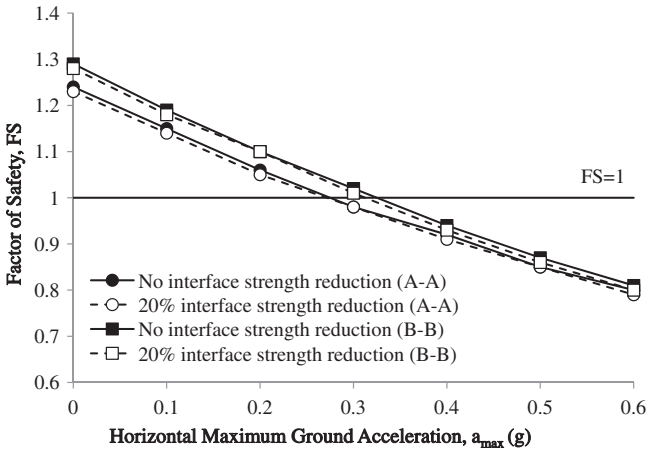

Fig. 14. Variation of FS with different horizontal peak ground accelerations for the 1999 slope failure at Sections A-A and B-B.

the slope stability of the reinforced slope at Section A-A for the 1994 slope failure, assuming two scenarios: 1. cohesion reduction in gravel–clay interface; 2. cohesion reduction in all soils. Fig. 11 shows the variation of FS with different percentages of cohesion reduction. Fig. 12 presents the FS contour and the most critical failure surface (white curve), gendered by ReSSA, at dry condition (i.e., no soil cohesion reduction). The limit equilibrium results show the FS = 1.01 at dry condition and decrease to FS = 0.96 at wet condition (i.e., 100% cohesion reduction in interface). FS become further less than 1.0 if 100% cohesion reduction in all soils is assumed. These analytical results suggest the slope was on the margin of instability after the excavation of original nature slope. Further reduction of soil cohesion due to moisture migration would cause the final collapse of the excavated and unprotected slope.

Fig. 13 shows the contour of maximum shear strain increment obtained from finite difference analyses. The finite difference results reveal that the slope failure was attributed to the stress concentration at the laterite gravel/clay interface. Failure started with a large shear strain that increased at the toe boundary of the lateritic gravel/clay interface and then propagated back into the natural slope until a shallow slide developed. In addition, it can be seen that the critical failure surface identified by the limit equilibrium analysis in Fig. 12 is comparable to the location of maximum shear strain increment by the finite difference analysis in Fig. 13.

Table 3
Limit equilibrium analysis results of Sections A-A and B-B.

Section	Reinforced slope height (m)	FS static analysis	Yield acceleration for FS = 1.0
A-A	40	1.24 (1.23)	0.27 (0.27)
B-B	30	1.29 (1.28)	0.32 (0.32)

Note: values inside the parenthesis indicate the results of considering 20% interface shear strength reduction.

Overall, the excavated and unprotected slope coinciding with high antecedent rainfall was the major cause to this year's landslide. Slope excavation during construction of the reinforced structure caused the daylight of this interface to have an unfavorable dip. What is worse, the long lasting raining season released large quantities of rainfall in the construction site, where no measures were taken to prevent rainfall infiltration or to drain the infiltration out of the soil. The interface soil was softened by a long season of rainfall infiltration, resulting in the reduction of soil shear strength and the final failure of the reinforced slope, as shown in the numerical analyses.

6.2. Results of 1999 slope failure analyses

Pseudo-static analyses were conducted using ReSSA to analyze the seismic stability of the reinforced slope for the 1999 slope failure at Sections A-A and B-B. Two scenarios were assumed: 1. no interface shear strength reduction; 2. 20% interface shear strength reduction under seismic loadings. Horizontal maximum ground accelerations a_{max} from 0.1 g to 0.6 g were input as the dynamic loading. As suggested in FHWA (2001), the horizontal acceleration inside the reinforced slope, a_h, equals to one half of the horizontal peak ground acceleration (i.e., $a_h = a_{max}/2$) was adopted in the analyses. Vertical acceleration is not considered in the analyses, assuming the peak vertical and horizontal accelerations do not happen simultaneously. The pore water pressures were ignored, because there had been no piping, seepage, or moisturized soil stratification in the field observation. Fig. 14 show the variation of FS with different horizontal maximum ground accelerations. The FS contour and the most critical failure surface at Section A-A are presented in Fig. 15. Table 3 summarizes the results of the pseudo-static analyses.

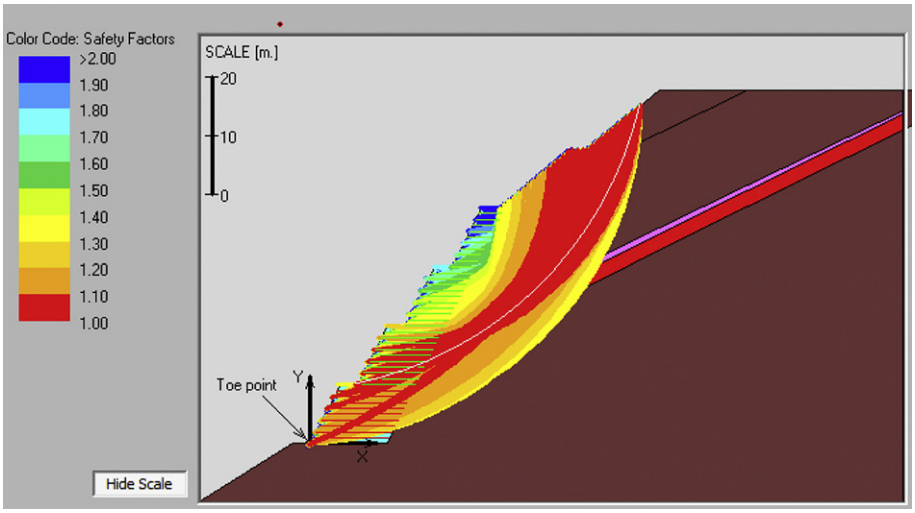

Fig. 15. FS contour and the most critical failure surface of the 1999 slope failure at Section A-A (no interface shear strength reduction and a_{max} = 0.3 g).

Specific important findings are discussed as follows. First, Fig. 14 suggests that the difference between 20% interface shear strength reduction and no reduction is insignificant (less than 1% difference in FS) for the global failure mode identified by the limit equilibrium analyses. The effect of interface shear strength reduction may be important for the direct sliding model along each reinforcement layer. This failure mode was also examined using ReSSA. However, it appears that the most critical mode is the global failure as reported in this study rather than the direct sliding. Second, the analysis results show the slope stability decreases with the increasing a_{max}. The slopes are initially stable under static condition (i.e., FS = 1.24 and 1.29 for Sections A-A and B-B, respectively) and then turn into instable (i.e., FS = 1) at a yield acceleration of 0.27 g for Section A-A and 0.32 g for Section B-B. That means, when the a_{max} greater than the yield acceleration applied on Sections A-A and B-B, the slopes would start to move.

The deformation behavior of the reinforced slope during the Chi-Chi earthquake was studied by performing dynamic analysis using FLAC. A minimum damping ratio of this system was assumed to be 5%, as suggested on the users' manual of FLAC code. The natural frequency of this site was calculated as 5 Hz according to the approach presented by Krizhner and Rosenhouse (2000). The subsurface borehole information and the recorded horizontal ground acceleration history at Station TCU074 was input into SHAKE program for simulating the ground motion at the base of this site. This history of ground motion was input into FLAC analysis as the dynamic loading in the finite difference analysis. The analysis duration was 90 s and the loads were applied every 0.1 s. Fig. 16 shows the shear strain distributions at Section A-A corresponding to different times.

In general, no significant permanent shear stain was observed in the early stage (before 20 s). When large horizontal ground

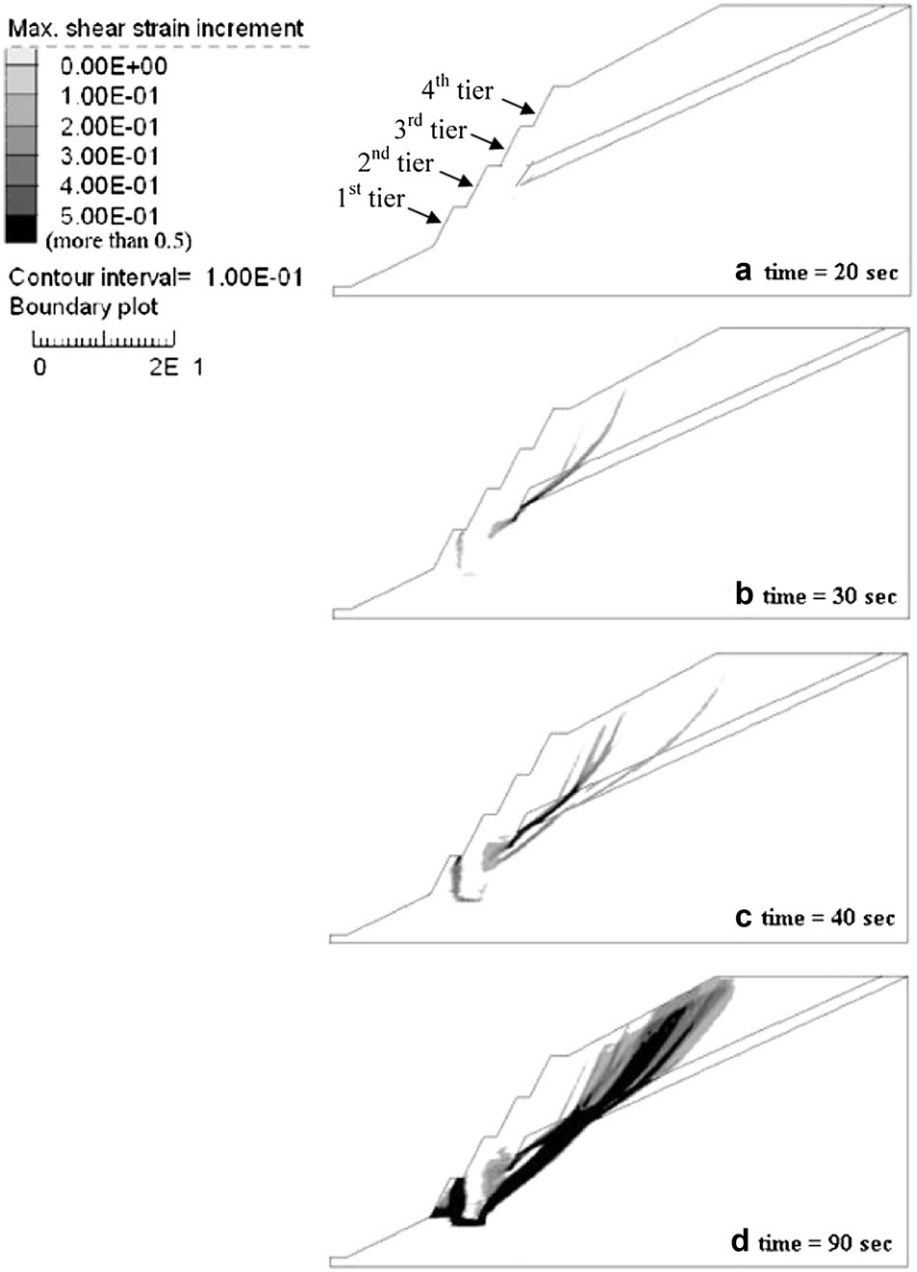

Fig. 16. Shear strain distributions at Section A-A for different times: (a) 20 s; (b) 30 s; (c) 40 s; (d) 90 s.

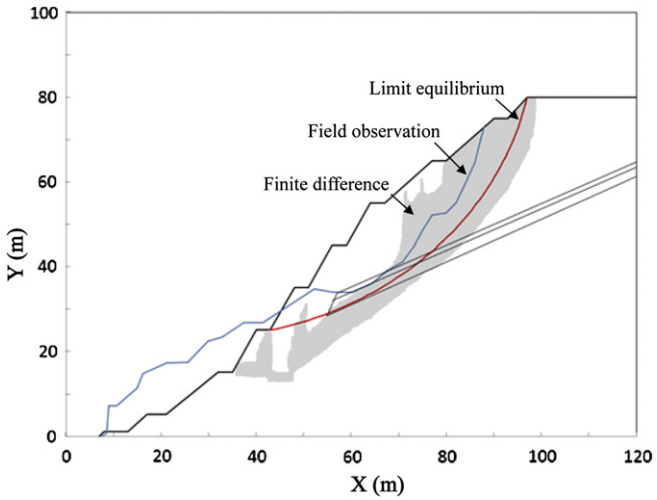

Fig. 17. Comparison of failure surface locations of the 1999 slope failure at Section A-A.

acceleration occurred at about 30 s, shear strain began to initiate at the back of the backfill zone (Fig. 16b). The stress increment concentrated at zones connecting backfill, clay layer, and natural laterite gravel. This showed that the stress concentration phenomenon is significant at the point where different materials gather. As the magnitude of earthquake loading increased with time, the induced shear strain within the slope increased accordingly. For example, at 40 s when peak ground acceleration occurred, the distribution of induced shear strain was more significant (Fig. 16c). The zone and magnitude of induced shear strain kept enlarging until 90 s (Fig. 16d) when there was no more massive ground acceleration. This clearly illustrates an external failure in that most of the shear strain was concentrated at the region where the backfill zone and the natural soil zone connected and compares well with the observed failure scarp as shown in Fig. 2. Fig. 17 shows the comparison of failure surface locations for the 1999 slope failure at Section A-A. Three failure surfaces from field observation, limit equilibrium analysis and finite difference analysis match reasonably well.

Last, additional analyses were conducted to examine the internal stability of the reinforced slope under seismic loadings. The analysis procedure followed the FHWA design guidelines (2001). The tensile failure and pullout mechanism of geogrid was checked for each layer. The analytical results suggested the slope did not fail internally due to reinforcement breakage or pullout. The results from pseudo-static analyses and the internal stability analyses confirm that the failure observed in the field was closely related to global instability. Overall, the major problem of the 1999

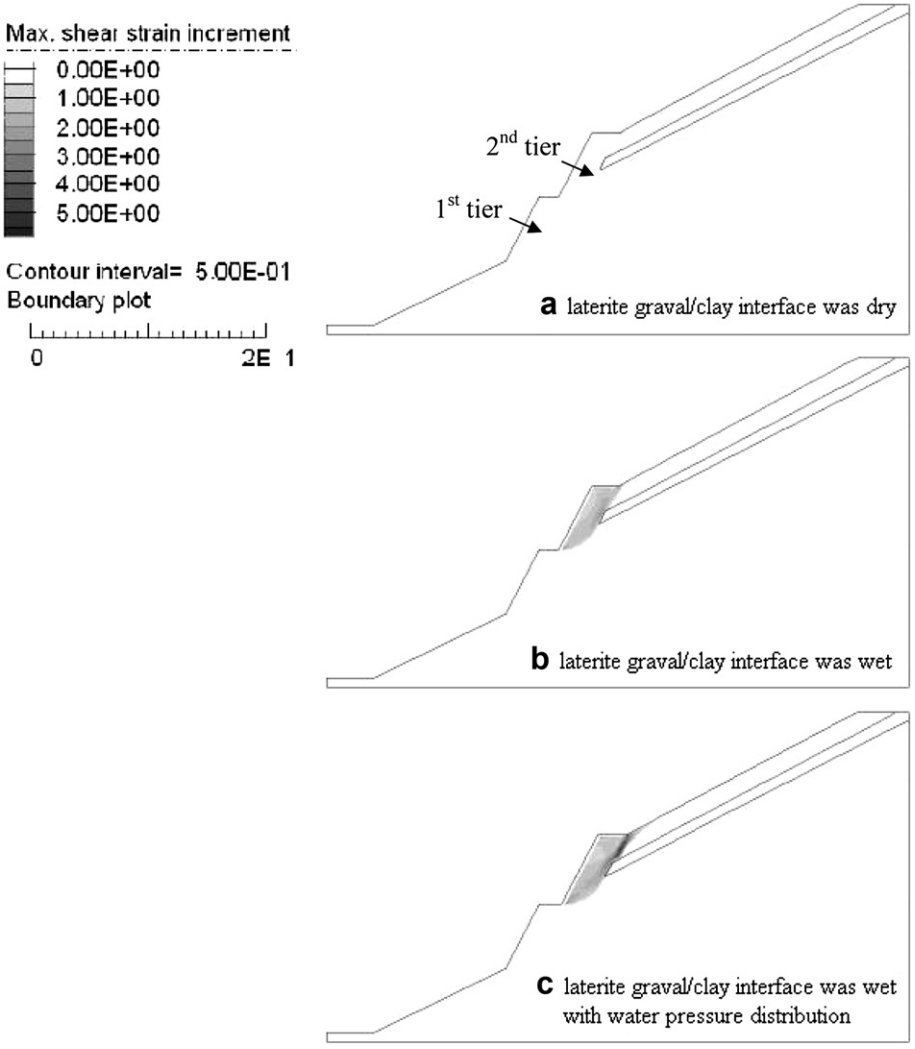

Fig. 18. FLAC analysis results of three scenarios for the 2004 slope failure at Section C-C: (a) dry interface; (b) wet interface; (c) wet interface with water pressure distribution.

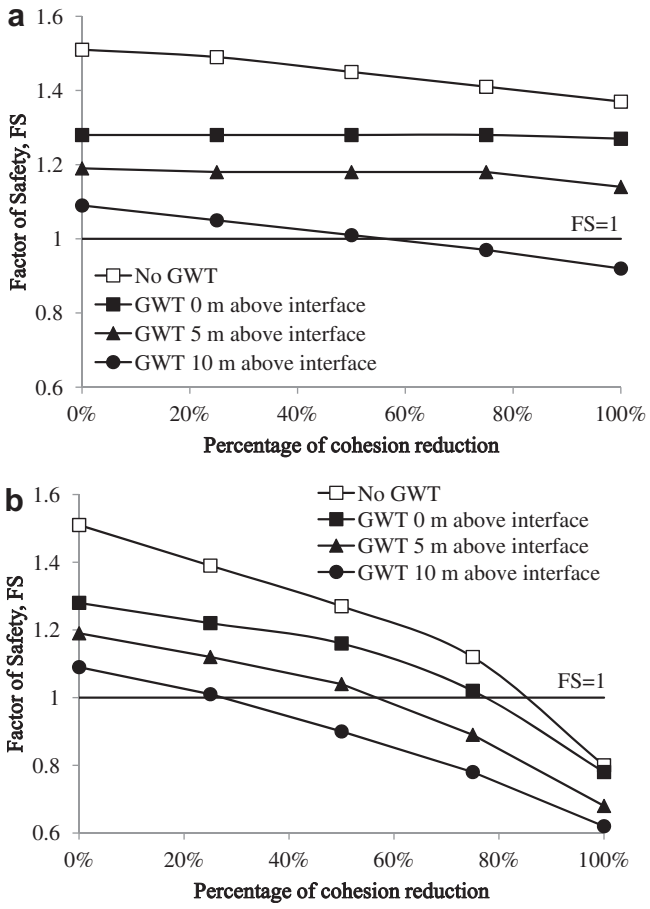

Fig. 19. Variation of FS with different percentages soil cohesion reduction and GWT levels for the 2004 slope failure at Section C-C: (a) cohesion reduction in interface; (b) cohesion reduction in all soils.

slope failure was due to the excessively strong ground accelerations during Chi-Chi earthquake. The slope failure was considered inevitable because the maximum ground acceleration during Chi-Chi earthquake was much greater than the design value as regulated in Taiwan.

6.3. Results of 2004 slope failure analyses

Considering the failure occurred after heavy rainfall from Typhoon Ming-Du-Li, the transient water pressure distributions during the heavy rainfall appeared to be critical in identifying the mechanism of failure, as high water pressure might have developed within the reinforced slope. Accordingly, transient seepage analyses using FLAC were performed to estimate the transient water pressure distributions within the slope. The soil permeability of the reinforced slope (Table 1) and the rainfall intensity and duration over this rainfall event were applied in the analyses. The results of transient seepage analyses showed as rainfall infiltrated into the retained slope, the water accumulated along the top of impermeable clay layer and behind the less permeable backfill zone. The water pressure distributed from 0 kPa at slope face to a maximum value approximately of 40 kPa along the top of clay layer.

In the subsequent finite difference analyses, three scenarios were investigated: laterite gravel/clay interface was dry, wet, and wet with water pressure distribution. The analysis result shows that the shear strain increment within the slope is insignificant for the scenario of dry laterite gravel/clay interface (Fig. 18a). However, shear strength began to develop for the scenario of wet laterite gravel/clay interface (Fig. 18b). The shear strain increment accumulated at the boundary of the backfill zone and the retained zone where the transient water pressure was induced by the rainfall infiltration for the scenario of wet interface with water pressure distribution (Fig. 18c). The shear strain increment extended upslope along the back of the reinforced zone and then into the natural slope to form a shallow sliding surface.

Limit equilibrium analyses were also conducted to evaluate the slope stability for the 2004 slope failure at Section C-C. The pore water pressures were simulated using various ground water table (GWT) levels from 0 m to 10 m above the interface layer. Similar to the 1994 failure case, two scenarios were considered: 1. cohesion reduction in gravel–clay interface; 2. cohesion reduction in all soils. These two scenarios were to simulate the reduction of soil shear strength and the loss of apparent cohesion that possibly occurred in the field due to moisture migration and absorption. Fig. 19 shows the variation of FS with different percentages of cohesion reduction and GWT levels. The FS contour and the most critical failure surface are presented in Fig. 20.

The analysis results show the slope stability decreases with the increasing GWT level and the reduction of soil cohesion. The slope

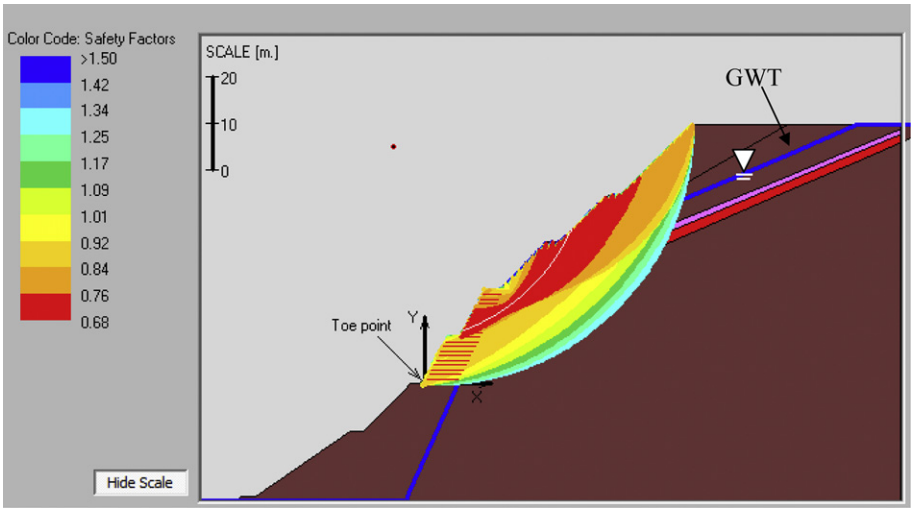

Fig. 20. FS contour and the most critical failure surface of the 2004 slope failure at Section C-C (100% cohesion reduction in all soils with GWT level 5 m above interface).

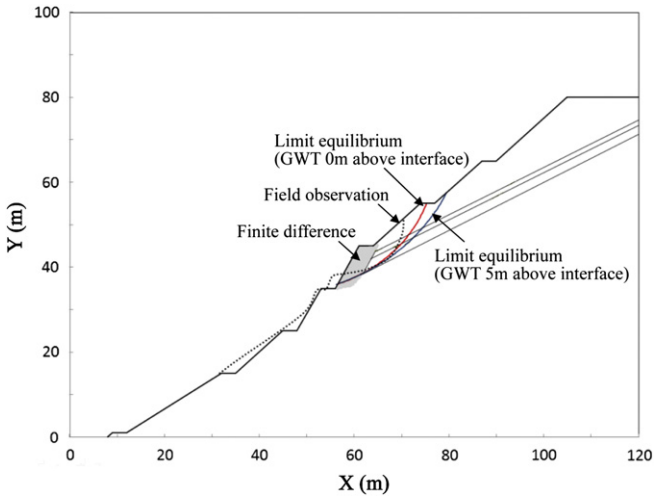

Fig. 21. Comparison of failure surface locations of the 2004 slope failure at Section C-C.

is initially stable (i.e., FS ≈1.5) at no ground water table and no soil cohesion reduction. The slope develops to be instable (i.e., FS = 1) when the GWT level and the percentage of soil cohesion reduction reach a certain combination. Limit equilibrium results, shown in Fig. 19, can justify that the assumption of cohesion reduction in all soils is closer to the real field condition. That is because failure of the reinforced slope (FS <1) occurs in the scenario of cohesion reduction in all soils when the GWT level is 5 m or less above the interface. The 5-m of GWT level above the interface in the limit equilibrium analyses can produce the water pressure distribution similar to the value calculated from the transient seepage analyses. However, there is no slope failure occurs in the scenario of cohesion reduction in interface; the result based on the assumption of cohesion reduction in interface contradicts to the field observation. Fig. 21 shows the comparison of failure surface locations. The locations of failure surfaces from field observation and limit equilibrium analysis match reasonably well but differ from that from finite difference analysis. The possible reason is because it is difficult to model the pore water pressure distribution in the field accurately. It also can be observed in Fig. 21 that the failure surfaces searched by limit equilibrium analyses are sensitive to the GWT level.

Overall, the analytical results indicate that the failure was attributed to heavy rainfall and the poor subdrainage defect. A significant amount of rainfall infiltrated into the retained slope, which had a hydraulic conductivity in the order of 10^{-3} cm/s. The infiltration not only softened the laterite gravel/clay interface, but because no subdrainage was constructed in the geosynthetic slope, the infiltration accumulated above the impermeable clay layer and behind the less permeable backfill zone to stimulate a significant value of transient water pressure. The perched infiltration tends to induce instability of the interface between gravel and clay, consequently inducing slope failure.

7. Discussions and conclusions

Three failures of a geosynthetic slope occurred over a duration of 10 years (1994–2004) in central Taiwan. This paper offers information including geometry, design, field observation, geological and material property tests, and numerical analyses. The first slope failure occurred in 1994 after a long rainy season. Rainfall infiltrated into the permeable laterite gravel and was impeded by the underlying impermeable clay layer. The interface of laterite gravel and clay created a detrimental bedding plane and its shear strength was reduced by the infiltration. A slide initiated from the interface occurred when the slope's toe was excavated to construct the reinforced zone. The second failure occurred in 1999 was caused by a very strong earthquake. The overstress initiated near the vicinity of the clay layer, retained zone, and reinforced zone. The overstressed zone dissipated into a retained natural slope to form a mass slide. The third failure occurred in 2004 when abundant rainfall infiltrated into the reinforced slope during a heavy rainstorm. Because no subdrainage system was designed, the infiltration that was obstructed by the impermeable clay and fine contents in the backfills began to generate significant transient water pressure, subsequently inducing slope failure behind the reinforced zone.

Aside from adverse environmental causes, such as a strong earthquake and heavy storms, these failures were also attributed to the existence of a clay layer. The interface between laterite gravel and clay is an embedded weak plane, especially when moisturized, it become softened. In addition, because of low permeability, it was also a barrier to the infiltration. The site investigation failed to find the existence of this clay layer, because the reinforced slope was thought to be subsidiary to campus buildings, and thus there were no investigation efforts made specific to the reinforced structures. The series of slope failures started out with poor site investigation. The succeeding design and construction did not appropriately correspond to this clay layer even when it was observed during construction. The adverse influences of the clay layer, such as soil cohesion reduction due to moisture migration, on the stability of the reinforced slope system were evaluated in this study. The results showed the impact of the clay layer on the slope stability was very critical. The results also suggested the current practice in the countries like Taiwan, where soil cohesion is used in design of earth structures, should not rely on the soil apparent cohesion in design because this apparent cohesion may easily decrease or even vanish with the increasing soil saturation.

The lack of a subdrainage system was another significant mistake in this case. It is a common practice in many sites to use soil available in the field that does not have fully satisfactory physical properties. For the backfills that contained a high percentage of fines and have low permeability, an appropriate installation of drainage systems is essential to stability. This case history highlights that neglecting basic geotechnical engineering principles can result in a major failure or even a series of failures.

Another lesson learned from the case history is the necessity to evaluate the global stability. The reinforced system might have a high factor of safety for separate individual walls, but a low factor of safety for the global system for the most critical sliding place to pass through the retained region. As seen in this paper, the stability performance of the reinforced zone performed successfully, because of the well developed design requirement and widespread experiences. However, the global stability for this high reinforced slope, which is a function of geometry and mechanical characteristics of the retained zone, is usually more critical. It is essential to consider not only the stability of the reinforced zone itself, but also that of the total system including the adjacent topography.

The last lesson learned from the case history is to combine the design of a high, steep reinforced slope with other types of retaining structures to improve the system stability. With the application of reinforced material on roadways in mountainous regions becoming more prevalent, the application of geosynthetic reinforcement in a high slope may not be optimal after considering the cost associated with a long embedded length, especially to prevent the global failure occurred. The incorporation of geosynthetic reinforcement and other reinforcing components, such as nailing and tapering as applied in the rehabilitated slope after the 1999 Chi-Chi earthquake, is an alternative for the design of a steep,

high reinforced slope system. Several detrimental environmental conditions occurred after the reinforced slope was rehabilitated following the 1999 Chi-Chi earthquake. Aside from Typhoon Ming-Du-Li which induced the 2004 failure, Typhoon Morakot on August 8, 2009 brought heavy rainfall again to this site (three-day rainfall accumulation of 663.5 mm was recorded at a nearby precipitation station), and a strong earthquake of magnitude 6.2 that occurred on November 5, 2009 at Mingjen (about 27 km from the case site) also induced a maximum ground acceleration of 154 gals in the E–W direction. The rehabilitated slope performed well under these critical events, as no trace of instability was observed.

Nomenclature

a_h	horizontal maximum acceleration inside the reinforced slope (g)
a_{max}	horizontal maximum ground acceleration (g)
c'	soil cohesion (kN/m^2)
c_a	interface cohesion between geogrid and soil (kN/m^2)
J	geogrid stiffness (kN/m)
G	soil shear modulus (kN/m^2)
k	soil hydraulic conductivity (cm/s)
K	soil bulk modulus (kN/m^2)
K_s	interface shear stiffness between geogrid and soil (kN/m^3)
t	geogrid thick (m)
T_{ult}	ultimate tensile strength of geogrid (kN/m)

Greek letters

δ	interface friction angle between geogrid and soil (kN/m^2)
ϕ'	soil friction angle (°)
γ_t	total unit weight of soil (kN/m^3)
σ_n	normal stress (kN/m^2)

References

AASHTO, 2002. Standard Specifications for Highway Bridges, seventeenth ed. American Association of State Highway and Transportation Officials, Washington, DC, USA, 689 pp.

Borges, J.L., Cardoso, A.S., 2002. Overall stability of geosynthetic-reinforced embankments on soft soils. Geotextiles and Geomembranes 20 (6), 395–421.

Chang, D.T., Chen, T.C., Su, K.H., 1991. "Utilization of geotextile-reinforced retaining wall for stabilizing weathered mudstone slope." In: Proceedings of Geosynthetics. vol. 91, Atlanta, GA, pp. 739–753.

Chen, R.H., Liu, C.N., Chen, K.S., Chen, T.J., 2000. Analysis of a reinforced slope failure induced by the Chi-Chi (Taiwan) earthquake. Journal of the Chinese Institute of Engineers 23 (4), 429–437.

Chou, N.S., Fan, C.C., 2000. "Failure investigation of the reinforced slope at the National Chi-Nan University during the 1999 Chi-Chi earthquake." In: Intl. Workshop on Annual Commemoration of Chi-Chi Earthquake, Taipei, Taiwan, pp. 178–189.

Collins, J.G., 2001. Lessons learned from a segmental retaining wall failure. Geotextiles and Geomembranes 19 (7), 445–454.

Duncan, J.M., Byrne, P., Wong, K.S., Mabry, P., 1980. Strength, Stress-strain and Bulk Modulus Parameters for Finite Element Analyses of Stresses and Movement in Soil Masses. Geotechnical Engineering Report No. UCB/GT/80-01. University of California, Berkeley, 70 pp.

Federal Highway Administration, 2001. Mechanically Stabilized Earth Walls and Reinforced Soil Slopes-design and Construction Guidelines. FHWA-NHI-00–043, U.S.A.

Holtz, R.D., Kramer, S.L., Hsien, C.W., Huang, A.B., Lee, W.F., 2001. "Failure analysis of an 80 m high geogrid reinforced wall in Taiwan." In: Proceedings of 15th International Conference on Soil Mechanics and Geotechnical Engineering, Istanbul, Turkey, pp. 1159–1162.

Huang, C.C., Horng, J.C., Chang, W.J., Chiou, J.S., Chen, C.H., 2011. Dynamic behavior of reinforced walls – horizontal displacement response. Geotextiles and Geomembranes 29 (3), 257–267.

Huang, C.C., 2000. "Performance of reinforced soil structures during Ji-Ji and Hanshin earthquakes, and slope reinforcement method of Japan high speed railways after the earthquake." In: Proceedings of Symposium on Latest Development of Reinforced Soil Retaining Structures, Taipei, Taiwan, pp. 70–102. (in Chinese).

Hung, J.J., 1978. Preliminary study of engineering properties of composite soil. Bulletin of the College of Engineering, National Taiwan University 23, 1–12 (in Chinese).

Itasca Consulting Group, Inc., 2000. Fast Lagrangian Analysis of Continua, Version 4.0, vols. I, II, III, IV.

Jewell, R.A., 1991. Application of revised design charts for steep reinforced slopes. Geotextiles and Geomembranes 10 (3), 203–233.

Jiang, C.H., 2006. "Case study of high steep reinforced slopes," Master thesis, Civil Engineering Department, National Chi-Nan University, 143 pp. (in Chinese).

Krizhner, F., Rosenhouse, G., 2000. Numerical analysis of tunnel dynamic response to earth motion. Tunneling and Underground Space Technology 15 (3), 249–258.

Lee, W.F., 2000. "Internal stability analyses of geosynthetic reinforced retaining walls," Doctoral dissertation, Civil and Environmental, University of Washington, Seattle, 381 pp..

Leonards, G.A., Frost, J.D., Bray, J.D., 1994. Collapse of geogrid-reinforced retaining structure. Journal of Performance of Constructed Facilities, ASCE 8 (4), 274–292.

Leshchinsky, D., Boedeker, R.H., 1989. Geosynthetic reinforced soil structures. Journal of Geotechnical Engineering, ASCE 115 (10), 1459–1478.

Leshchinsky, D., Hu, Y., Han, J., 2004. Limited reinforced space in segmental retaining walls. Geotextiles and Geomembranes 22 (6), 543–553.

Ling, H.I., Leshchinsky, D., Chou, N.N.S., 2001. Post-earthquake investigation on several geosynthetic-reinforced soil retaining walls and slopes during 1999 Ji-Ji Earthquake of Taiwan. Soil Dynamics and Earthquake Engineering 21 (4), 297–313.

Mandal, J.N., Joshi, A.A., 1996. Design of geosynthetic reinforced embankments on soft soil. Geotextiles and Geomembranes 14 (2), 137–145.

National Concrete Masonry Association, 2010. In: Bathurst, R.J. (Ed.), Design Manual for Segmental Retaining Walls, third ed., p. 282. Herndon, Virginia, USA.

Ponterosso, P., Fox, D. St. J., 1999. "Preliminary layout of reinforced earth embankments by genetic algorithm." In: Proceedings of the International Conference on Computational Methods and Experimental Measurements. pp. 603–612.

Raisinghani, D.V., Viswanadham, B., 2011. Centrifuge model study on low permeable slope reinforced by hybrid geosynthetics. Geotextiles and Geomembranes 29 (6), 567–580.

Rowe, R.K., Skinner, G.D., 2001. Numerical analysis of geosynthetic reinforced retaining wall constructed on a layered soil foundation. Geotextiles and Geomembranes 19 (7), 387–412.

San, K.C., Leshchinsky, D., Matsui, T., 1994. Geosynthetic reinforced slopes: limit equilibrium and finite element analyses. Soils and Foundations 34 (2), 79–85.

Scarborough, J.A., 2005, "A tale of two walls: case histories of failed MSE walls." In: Proceedings of Geo-Frontiers 2005. pp. 2751–2762.

Schmertmann, G.R., Chouery-Curtis, V.E. Johnson, R.D., Bonapart, R., 1987. "Design charts for geogrid-reinforced soil slopes." In: Proc., Geosynthetics' 87 Conf., New Orleans, La., pp. 108–120.

Tatsuoka, F., Tateyama, M., Koseki, J., 1995. "Behavior of geogrid-reinforced soil retaining walls during the Great Anshin-Awaji Earthquake." In: Proceedings of the First International Symposium on Earthquake Geotechnical Engineering. pp. 55–60.

Turner, J.P., Jensen, W.G., 2005. Landslide stabilization using soil nail and mechanically stabilized earth walls: case study. Journal of Geotechnical Engineering, ASCE 131 (2), 141–150.

Viswanadham, B., Konig, D., 2009. Centrifuge modeling of geotextile-reinforced slopes subjected to differential settlements. Geotextiles and Geomembranes 27 (2), 77–88.

Yoo, C., Jung, S.B., 2008. Performance of a two-tier geosynthetic reinforced segmental retaining wall under a surcharge load: full-scale load test and 3D finite element analysis. Geotextiles and Geomembranes 26 (6), 460–472.

Yoo, C., Kim, H.S., 2004. Measured behavior of a geosynthetic-reinforced segmental retaining wall in a tiered configuration. Geotextiles and Geomembranes 22 (5), 359–376.

Yoo, C., Jung, H.S., Jung, H.Y., 2004 "Lessons learned from a failure of geosynthetic-reinforced segmental retaining wall." In: Proceedings of 3rd Asian Regional conference on geosynthetics, Seoul, Korea, pp. 265–274.

Yoo, C., Jung, H.S., Jung, H.Y., 2006. Case history of geosynthetic-reinforced segmental retaining wall failure. Journal of Geotechnical and Geoenvironmental, ASCE 132 (12), 1538–1548.

Yoo, C., 2004. Performance of a 6-year-old geosynthetic-reinforced segmental retaining wall. Geotextiles and Geomembranes 22 (5), 377–397.